

701

Semi_detailed_survey_area

Geological Section Lines

Ore deposits and Prospects

- Porphyry-Cu
- Porphyry-Cu, Mo
- Porphyry-Cu, Au
- Vein and Irregular-Cu
- Vein-Mo
- Vein-Au
- Vein-Ag, Pb, Zn
- Vein-Sb
- Vein and Irregular-Fe
- Vein and Irregular-Mn
- Unknown-Cu
- Unknown-Au
- Unknown-Ag, Pb, Zn

Pb (geochem. + ore assay)

- 1023 - 46517 (ppm)
- 613 - 1022
- 233 - 612
- 49 - 232
- 1 - 48

Geomap_Putre_W

- Qal (Recent sediments)
- Qv (Quaternary-Tertiary volcanics)
- Qvr (Quaternary-Tertiary ignimbrite)
- TQc (Quaternary-Tertiary conglomerate)
- Tig (Miocene-Pliocene ignimbrite)
- Kc(i) (Cretaceous sediments)
- Intrusive rocks
- Tgd (Tertiary granodiorite)

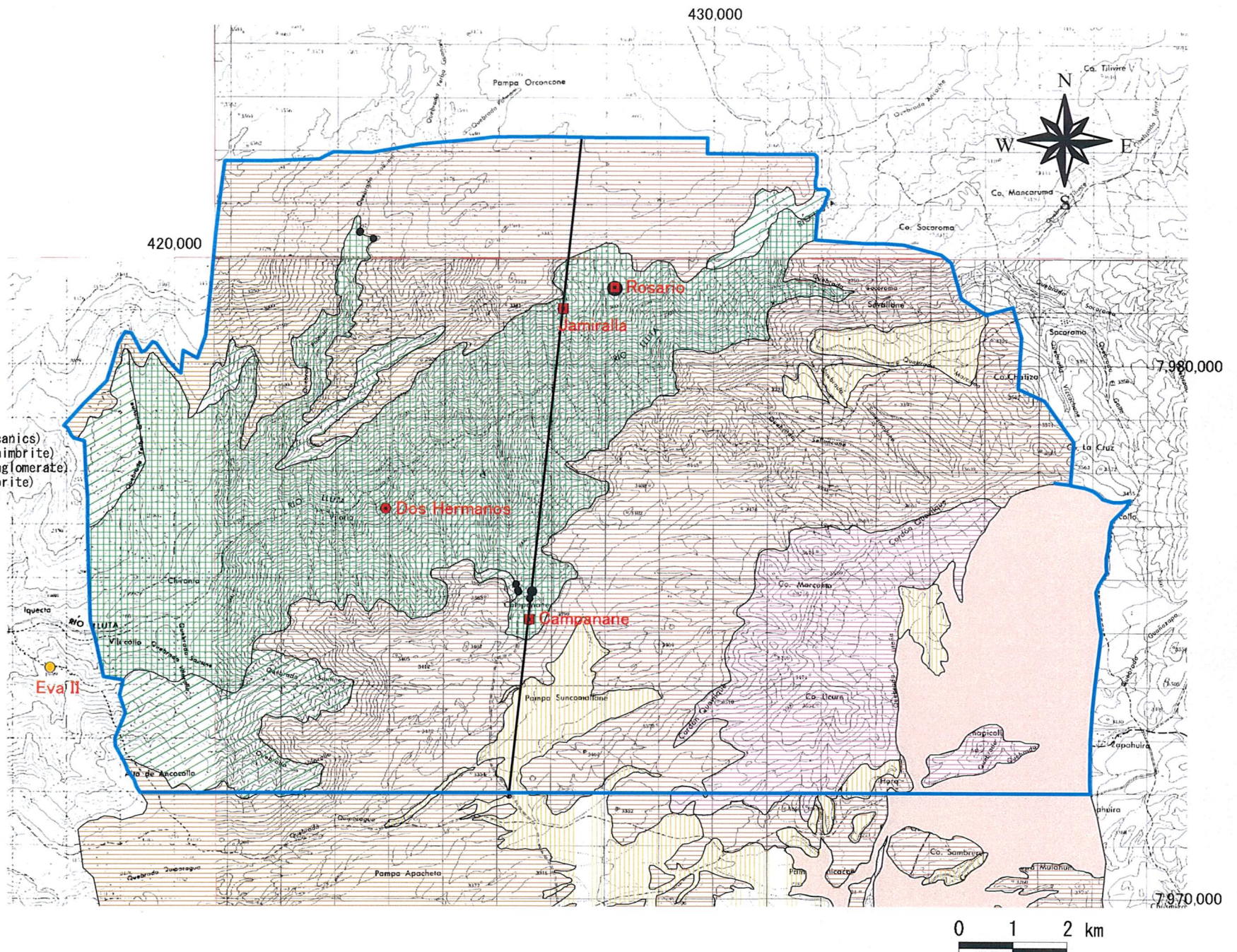


Fig. 2-2-99 (4) Geochemical Anomaly Map in the Area to the West of Putre (Pb)

471

Semi_detailed_survey_area

Geological Section Lines

Ore deposits and Prospects

- Porphyry-Cu
- Porphyry-Cu, Mo
- Porphyry-Cu, Au
- Vein and Irregular-Cu
- Vein-Mo
- Vein-Au
- Vein-Ag, Pb, Zn
- Vein-Sb
- Vein and Irregular-Fe
- ▲ Vein and Irregular-Mn
- Unknown-Cu
- Unknown-Au
- Unknown-Ag, Pb, Zn

Zn (geochem. + ore assay)

- 224 - 2005 (ppm)
- 143 - 223
- 74 - 142
- 29 - 73
- 1 - 28

Geomap_Putre_W

- Qal (Recent sediments)
- Qv (Quaternary-Tertiary volcanics)
- Qvr (Quaternary-Tertiary ignimbrite)
- TQc (Quaternary-Tertiary conglomerate)
- Tig (Miocene-Pliocene ignimbrite)
- Kc(i) (Cretaceous sediments)
- Intrusive rocks
- Tgd (Tertiary granodiorite)

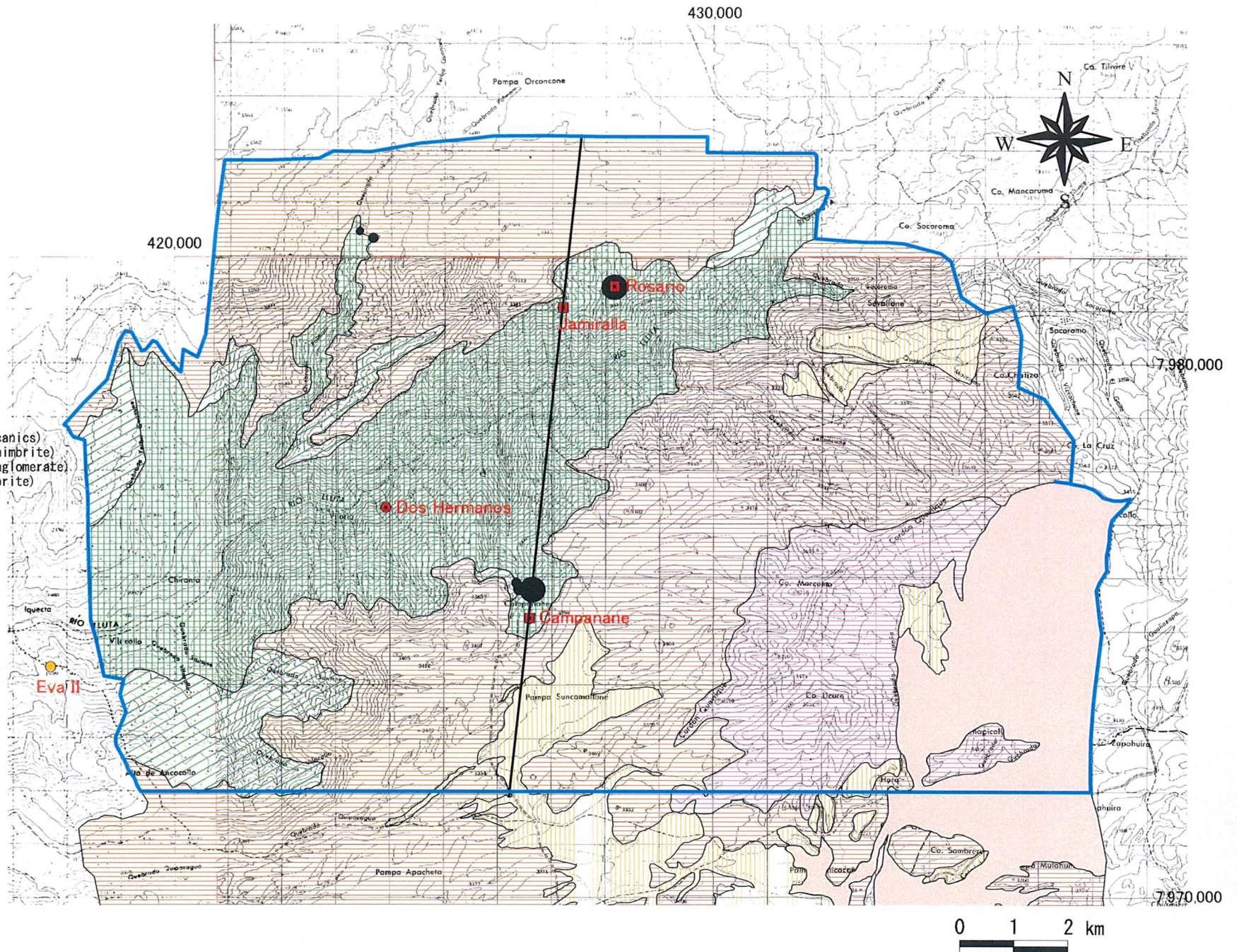


Fig. 2-2-99 (5) Geochemical Anomaly Map in the Area to the West of Putre (Zn)

In this area, vein-type copper mineralization (Campanane, Jamiralla, and Rosario Prospects) occur at three localities in granodiorite. The above prospects all consist of aggregates of copper-oxide-bearing quartz-tourmaline veins (maximum width 40cm), and they partly form network. The extension of these veins is NNW~NNE, and the Jamiralla, Rosario Prospects are located at the NNE extension of the Campanane Prospect. Chalcopyrite, pyrite, and chrysocolla occur in the Campanane veins. The vicinity of these prospects are altered by silicification and sericitization accompanied by potash feldspar and tourmaline in some places.

Au-Ag-Cu-Pb-Zn anomalies were detected by rock geochemical survey.

The above prospects are all located within a zone where intermediate airborne magnetic intensity zones and the peripheries of short wavelength low magnetic anomaly zones overlap. Medium wavelength anomaly zones do not occur in the prospective areas.

CHAPTER 3 GRAVITY SURVEY

3 - 1 Survey Method

3-1-1 Gravity measurements

Gravity measurements was made at 349 points using two sets of LaCoste model G gravity meter within an area of 538km² in the Camarones district. A helicopter was used for commuting to far-off locations in the eastern, southern, and western parts of the district. The number of stations measured using helicopter amounted to 150 which constitute 43% of the total.

The Chile University gravity base ($g=978,480.233\text{mgal}$) within the Arica Airport about 100km northwest of the survey area. was used for reference stations.

3-1-2 Leveling

Differential Global Positioning System (DGPS) was used for determination of the location and elevation of each station. Three sets of 4600LS GPS surveyers by Trimble Navigation Ltd., of USA were used. One was for the base station and two for measuring points.

The GPS base station was set at the extreme northwest point of the survey area about 3.5km southeast of Codpa. The location and elevation of the GPS base station were determined by GPS survey from the triangulation point "Garza" located about 17km west-northwest.

3-1-3 Density measurements of rock sample

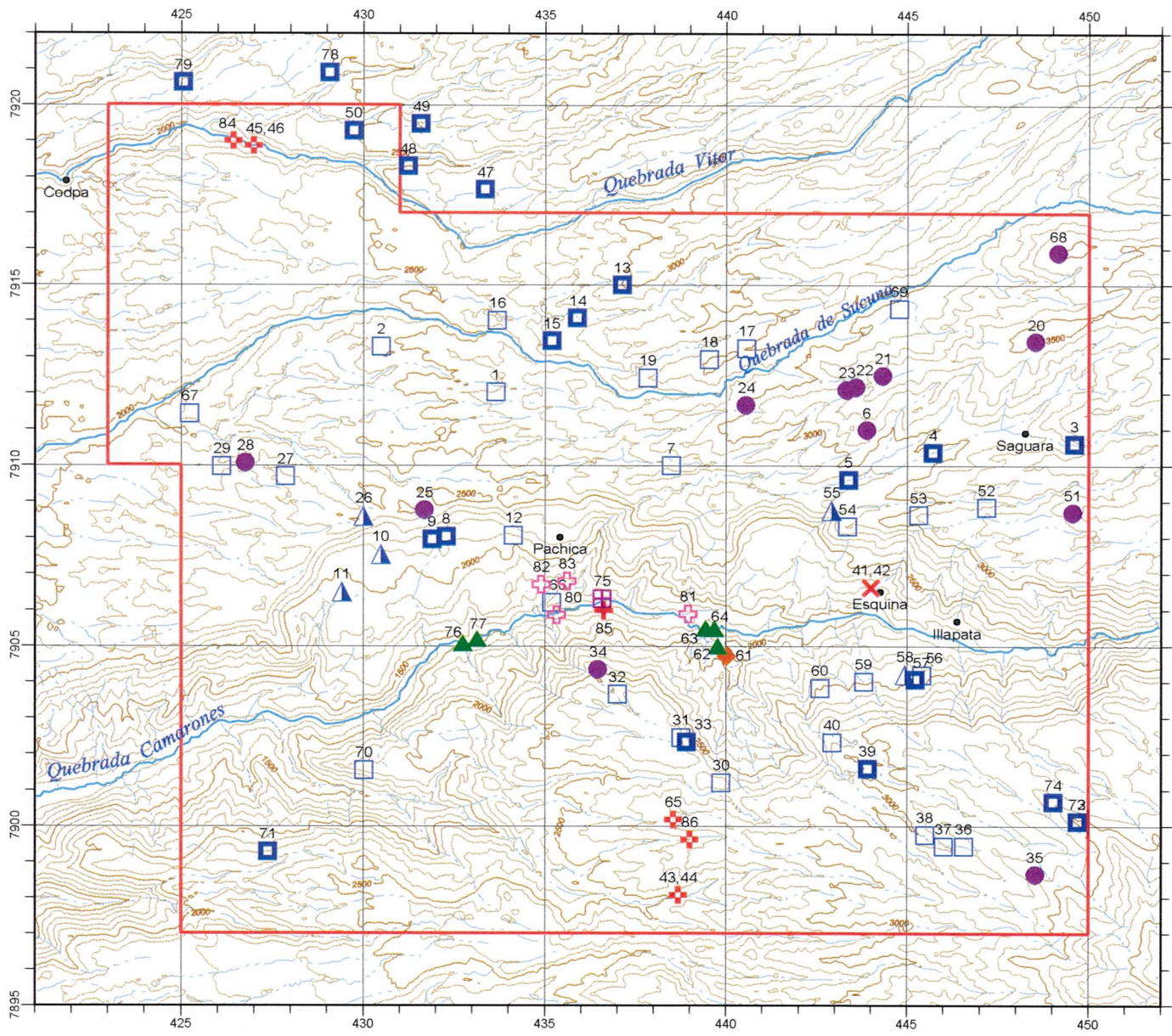
Density of 86 rock samples collected from the survey area was measured. The locality of the samples is shown in Figure 2-3-1. The average densities are shown for each formation and rock in Table 2-3-1.

It is seen from Table 2-3-1 that Quaternary agglomerate and Miocene ignimbrite forms the low-density group, while Quaternary basalt, basement rocks (Upper Cretaceous System, Upper Cretaceous-Paleogene System), and Cretaceous to Tertiary intrusive rocks form the high-density group. The difference between natural dry density and wet density of the low-density group rocks is 0.06~0.20g/cm³, and the effective porosity is relatively large. On the other hand, the difference between the natural dry density and the wet density is almost nil for high-density rocks and thus the effective porosity is very small.

The density of the rock samples is a basic data for determining the correction density in the

475

— 475 —



LEGEND

[Quaternary]

- Basalt
- ▲ Agglomerate

[Tertiary(Neogene)]

- Ignimbrite(Pumice tuff/
weakly welded tuff)
- Ignimbrite(Highly welded tuff)

[Cretaceous -
Early Tertiary]

- ◆ Rhyolitic volcanics
- ▲ Andesitic lava/
volcanics

[Cretaceous - Tertiary]

- ⊕ Granodiorite
- ⊗ Diorite porphyry
- ⊞ Diorite
- ⊕ Quartz porphyry
- ⊞ Quartz diorite

Fig. 2-3-1
Location of Rock Sample

terrain correction and Bouguer correction. Average density of the surface formations is important for determining the correction density. Ignimbrite is widely distributed in the Camarones district, and this rock has a wide density distribution from low-density pumiceous tuff to relatively high-density welded tuff. In such cases the actual density and simple average density may differ largely, and the average density must be calculated with consideration of the density distribution ratio. Considering the distribution ratio of [pumiceous tuff/lowly welded tuff] and [highly welded tuff] (inferred to be 2:8~1:9), the average naturally dry density becomes 2.23~2.28g/cm³ and the average wet density 2.32~2.35g/cm³. The dry or wet conditions of the subsurface zones of the Camarones district is not accurately known, but by adopting correction density of 2.23~2.35/cm³, reasonably accurate results should be obtained.

3 - 2 Results of the Survey

3-2-1 Gravity anomaly maps

(1) Bouguer anomaly map

Examinations on free air gradient and Bouguer density by Nettleton's profiles were carried out to determine a assumed density for Bouguer correction and terrain correction. Then a Bouguer anomaly map with free air gradient of 0.3000mgal/m and correction density of $\rho = 2.25\text{g/cm}^3$ shown in Figure 2-3-2 was prepared.

(2) Trend map and residual map

The Bouguer anomaly distribution of the survey area incorporates the gravity trend caused by the variation of the crust thickness. Therefore, the gravity trend must be deducted from the Bouguer anomaly map in order to prepare a gravity distribution map reflecting the subsurface structure of the survey area.

This is carried out as follows. First simply calculate the first order trend by using the 500m-interval lattice Bouguer anomaly values and prepare a first order residual map (Fig. 2-3-3(a), (b)) by deducting the calculated trend from the Bouguer anomaly map. The inclination of the trend obtained from above process was not exactly in the E-W direction, but in the WSW-ENE direction. The highest anomaly value in the residual map appeared in the northwesternmost part of the survey area, and not in the Quebrada Camarones zone where the basement rocks are widely distributed nor in the southernmost part of the area where existence of large-scale intrusive bodies is inferred. Figure 2-3-3 (b), therefore does not show gravity distribution harmonious with the distribution of geologic units.

The reason for the appearance of the maximum gravity anomaly value in the northwesternmost part in the residual map (Fig. 2-3-3 (b)) is the northern component of the calculated trend, WSW-ENE, and not E-W as the geology indicates. There is a NW-SE trend in the geologic structure of the Camarones district, and thus it is possible that the northern component of the trend reflects the geologic structure of the Camarones district and is not a regional component. Next the trend was re-calculated by limiting the direction of inclination to exactly E-W. The results are shown in Figure 2-2-11 (c) and (d). The residual map (d) shows the location of the maximum gravity anomaly value in the southernmost part of the survey area, and its gravity distribution is more harmonious with the geology compared to the map (b). Therefore Figure 2-3-3 (d) was used for analysis and interpretation. The Figure 2-3-3 (d) residual map is converted to 1:100,000 scale and shown in Figure 2-3-4.

The $\rho = 2.25\text{g/cm}^3$ residual map of Figure 2-3-4 shows distribution of high gravity anomalies at a wide zone from the eastern part to the southeastern and southern part of the survey area, westernmost part extending along the northwest margin to the southwest margin of the survey area, and the zone from middle reaches of Quebrada Camarones in the central part to the west of Pachica. On the other hand, low gravity anomalies occur in a wide zone from middle reaches of Quebrada Vitor to the middle reaches of Quebrada Sucuna in the northern part, southern bank of Quebrada Camarones in the southwest, and in the upper reaches of Quebrada Sucuna in the northeasternmost part of the survey area. A low gravity anomaly occurs over an area of $5\text{km} \times 5\text{km}$ in the southeastern part but this is a local occurrence and the southeastern part of the survey area is considered to be, on the whole, a high gravity zone. The low gravity anomaly between middle Quebrada Vitor and middle Quebrada Sucuna is characterized by a relatively high gravity trend in the eastern, southern, and western margins resulting in an anomaly zone with a clear outline.

The highest gravity anomaly value occurs near Station No.109 at the southernmost part of the area followed by the value near Station No.52 at the southwestern margin of the area. The lowest gravity anomaly value occurs near Station 197 in the northern part, and the second lowest value extends over an area of 3km E-W and 2km N-S on the southern bank of the middle stream of the Quebrada Sucuna.

The drainage zone of the Qubrada Camarones is almost all in the high gravity anomaly zone with the exception of a part of the southwestern part.

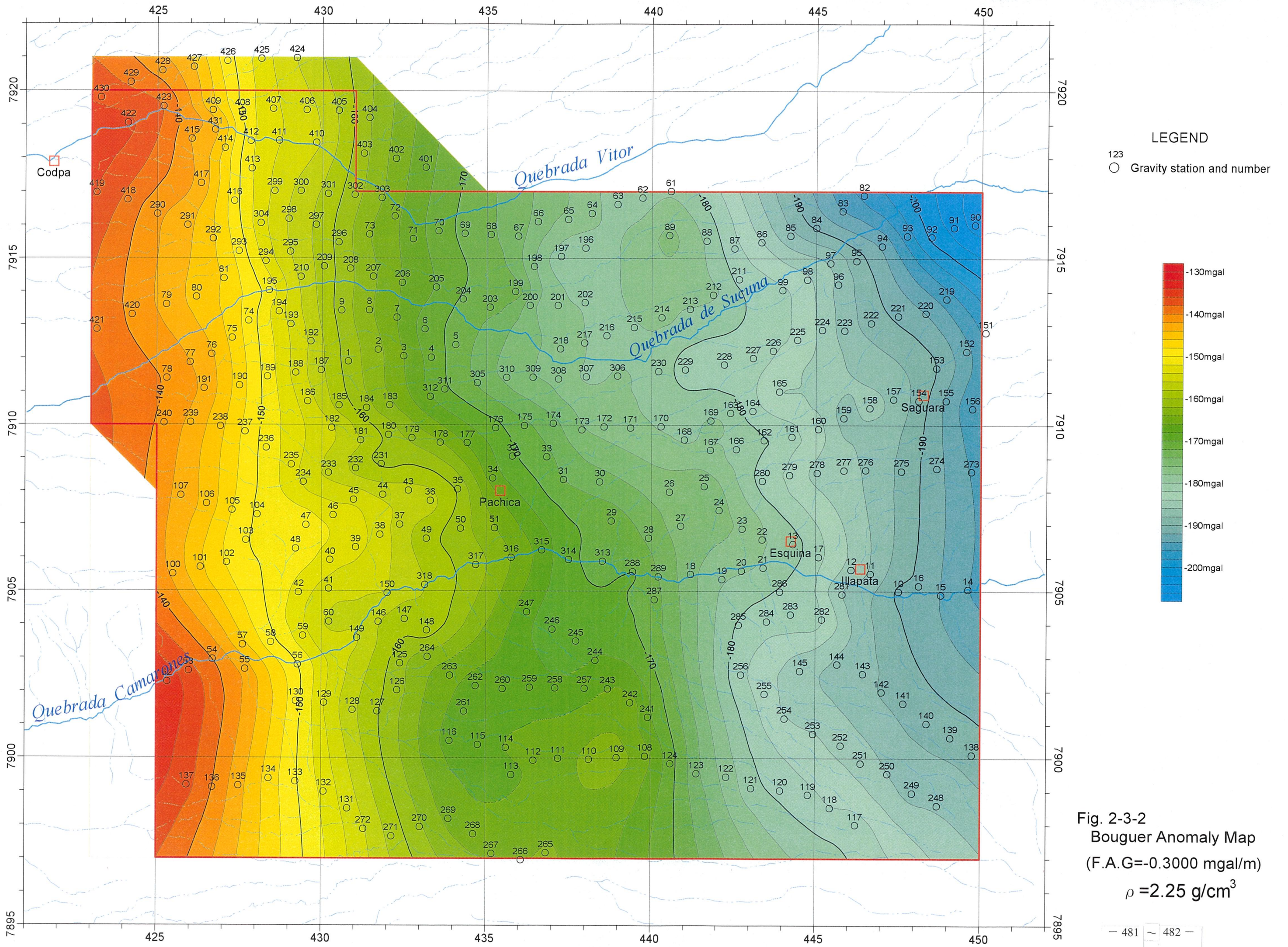
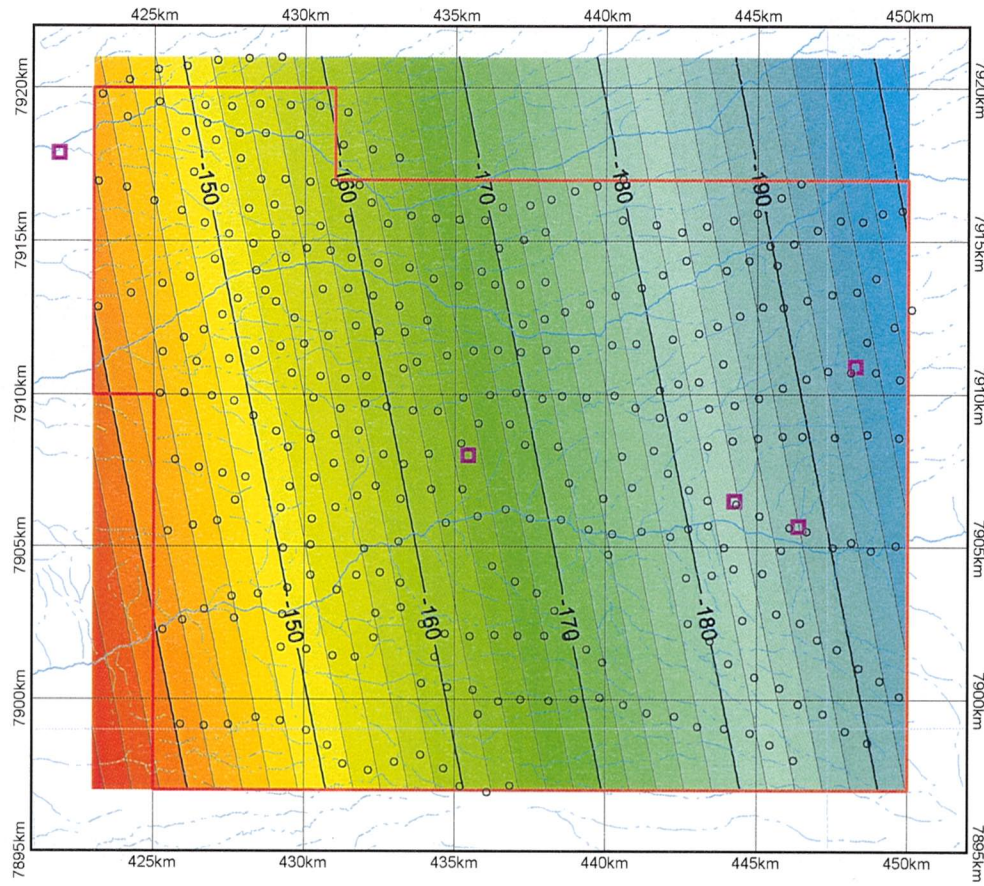
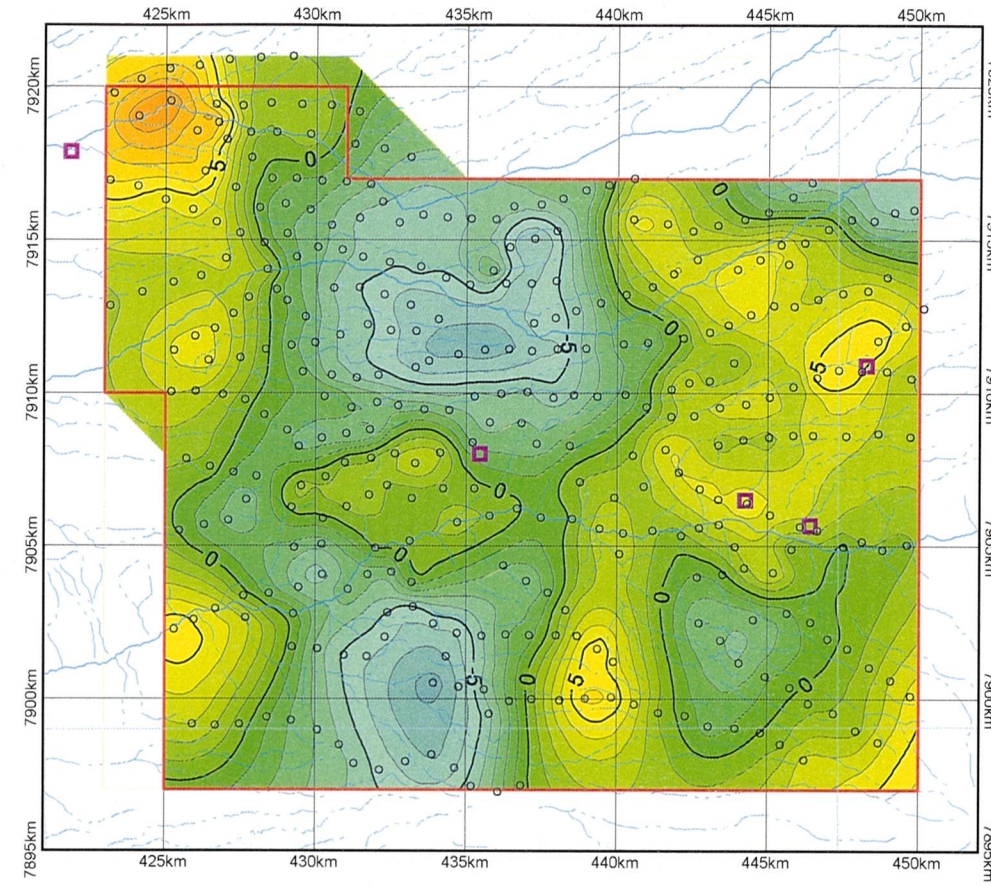


Fig. 2-3-2
 Bouguer Anomaly Map
 (F.A.G=-0.3000 mgal/m)
 $\rho = 2.25 \text{ g/cm}^3$

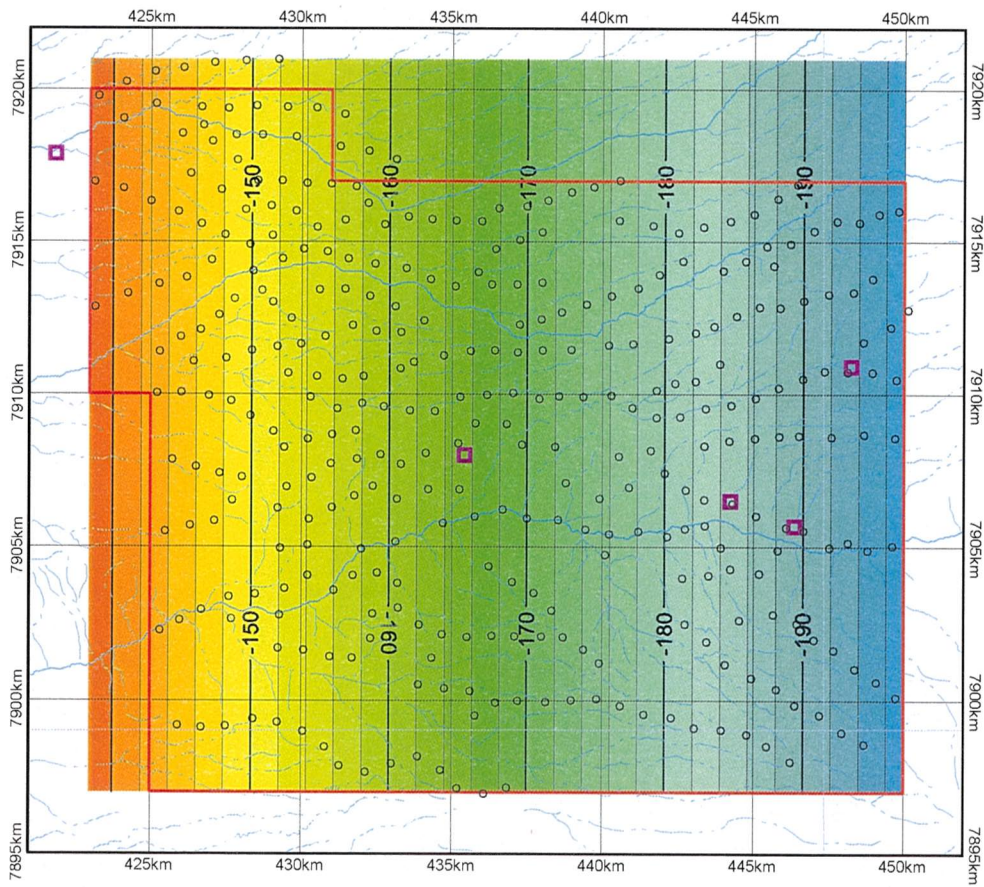
(a) First order trend(1)



(b) First order residual(1)



(c) First order trend(2)



(d) First order residual(2)

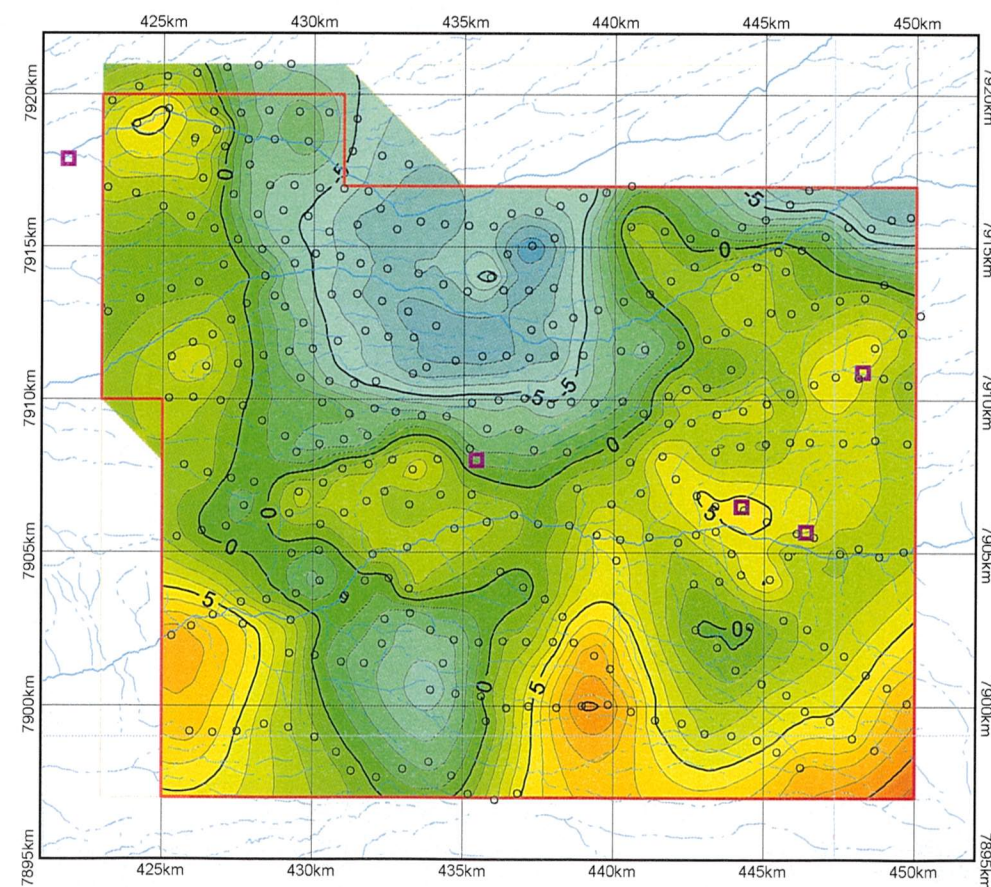


Fig. 2-3-3
Trend maps and Residual maps
(F.A.G = -0.3000 mgal/m)
($\rho = 2.25 \text{ g/cm}^3$)

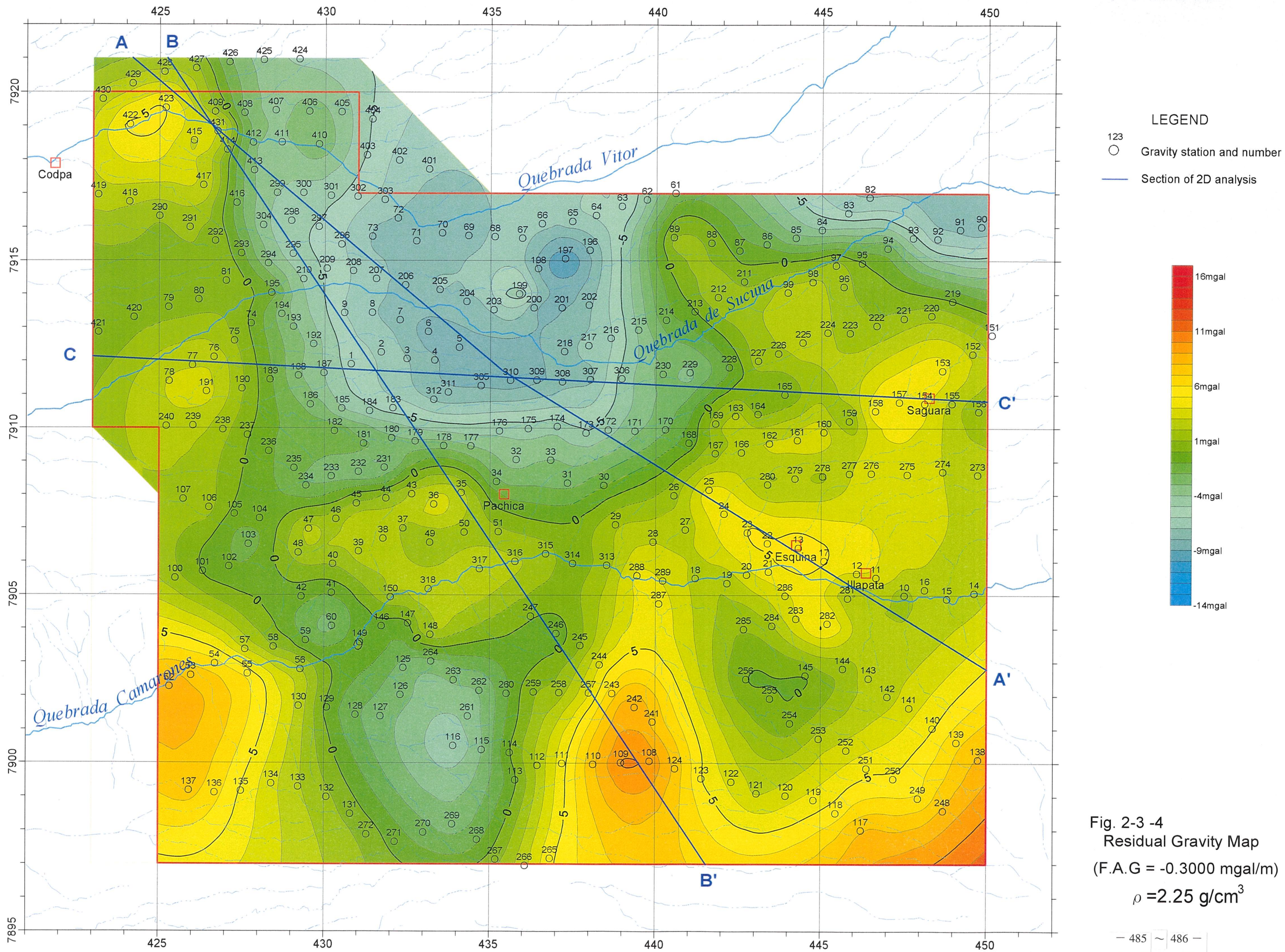


Fig. 2-3 -4
 Residual Gravity Map
 (F.A.G = -0.3000 mgal/m)
 $\rho = 2.25 \text{ g/cm}^3$

3-2-2 Gravity anomalies and aeromagnetic anomalies

Aeromagnetic map (Reduced to the pole map) of the Camarones district is shown in Figure 2-3-5. The magnetic map on the left side of Figure 2-3-5 is a reduced to the pole map before filtering, and that on the right side is a reduction to the pole map treated by a high-cut filter with wavelength threshold of about 2.5km. The magnetic maps before filtering is strongly affected by topography while the effect of topography is almost completely eliminated in the magnetic map after filtering.

Reduction to the pole map and residual gravity map are laid out in Figure 2-3-6 for examining the relation between gravity anomalies and magnetic anomalies. It is seen in this figure that low gravity anomalies correspond well with high magnetic anomalies in the northern to the central part of the area while high gravity anomalies and low magnetic anomalies correspond to each other in the eastern part. Also high gravity and high magnetic anomalies coincide well at two localities in the southernmost and northwestern margin of the area, and low gravity anomalies nearly coincide with low magnetic anomalies in the southwestern to the southern part.

The above is summarized as: "high gravity - high magnetic" and "low gravity - low magnetic" correlation occurs in regional anomalies while "high gravity - high magnetic" and "low gravity - low magnetic" relation exists for local-scale anomalies.

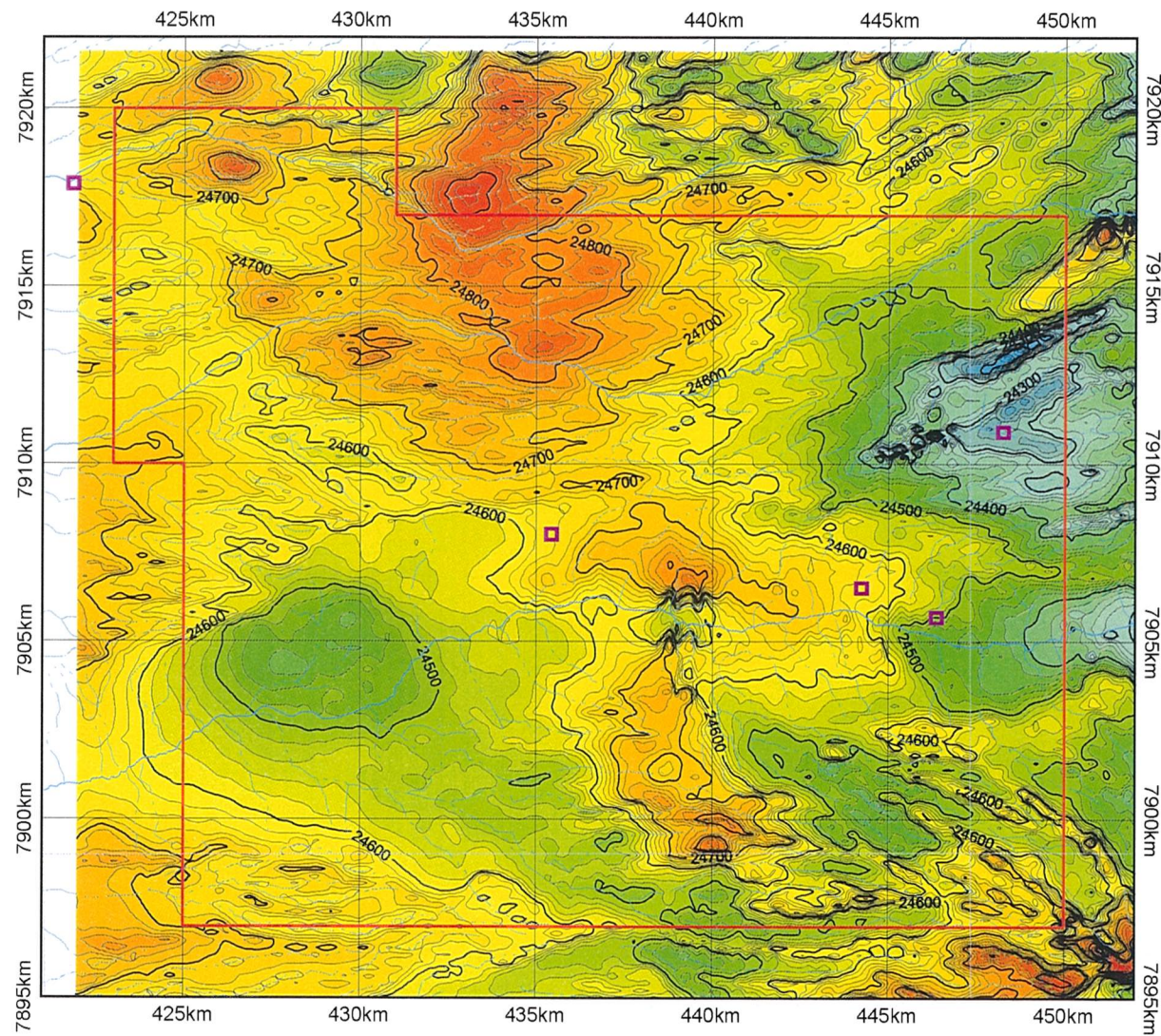
3-2-3 Two-dimensional analysis

Two-dimensional analysis was carried out for three profiles A-A', B-B', and C-C' of Figure 2-3-4. Analysis was done by two-layer modeling and multi-layer modeling and the results are shown in Figures 2-3-7~2-3-9. In these figures, measured and calculated gravity anomalies (residual gravity) values are listed in the top sections, two-layer modeling results in the middle, and the multi-layer modeling results in the bottom.

The measured gravity anomaly values are shown by red lines, the calculated gravity anomaly values by different symbols for two-layer modeling (3-density contrasts) and multi-layer modeling results (1-density contrast). Also magnetic anomaly (deduction to the pole) profiles along the same section are shown by blue lines for reference.

Two-layer modeling is an analytical method of examining the difference of the depth of the

(a) Non filtered



(b) High-cut filtered

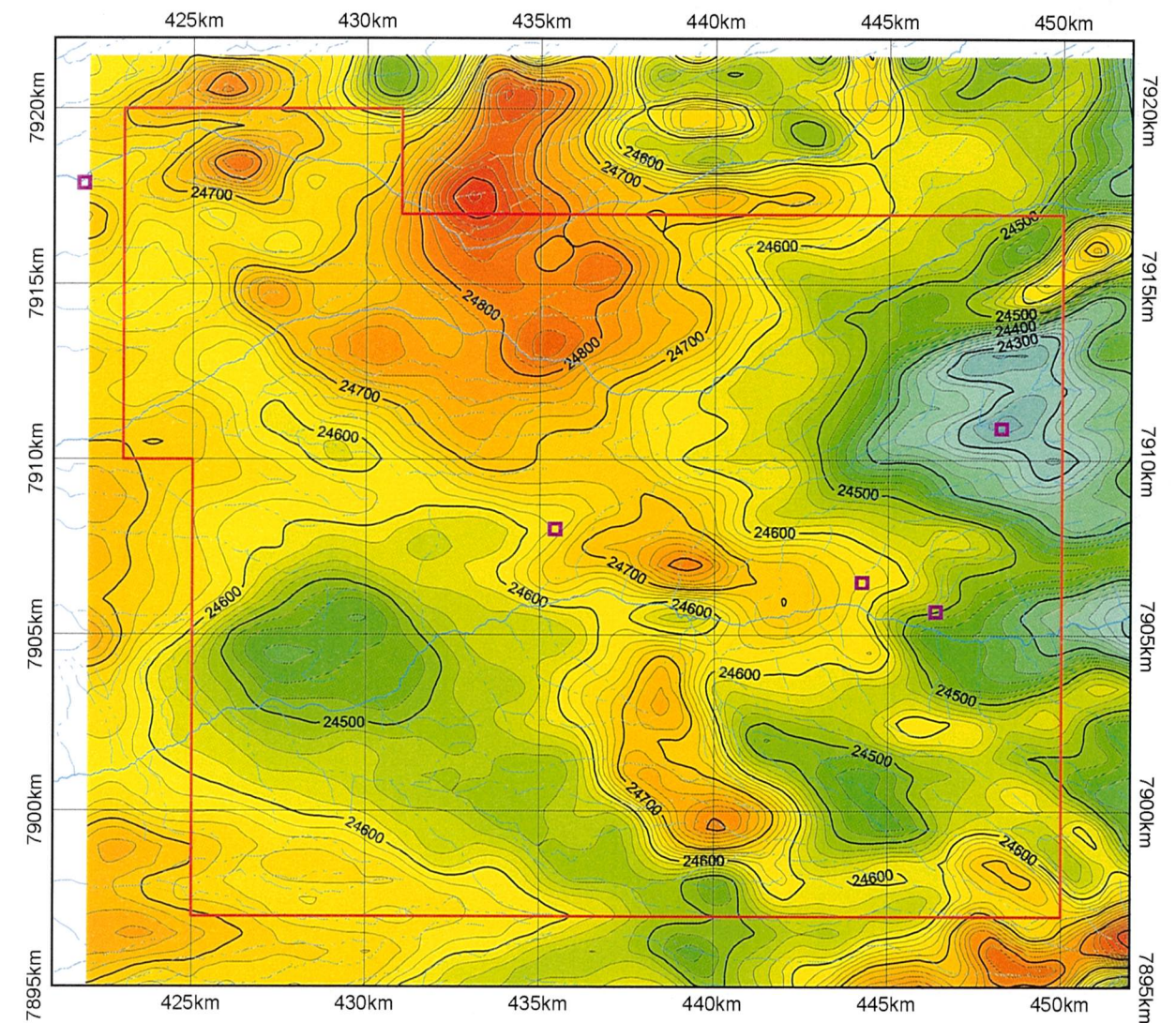


Fig. 2-3-5 Aeromagnetic Maps (Reduction to the pole)

489